

The Non-monotonicity of Moist-Adiabatic Warming

Osamu Miyawaki^a

^aDepartment of Geosciences, Union College, Schenectady New York, USA

1

2

3

⁴ Corresponding author: Osamu Miyawaki, miyawako@union.edu

5 ABSTRACT: The moist adiabat is a foundational model of moist thermodynamics that is used
6 to understand convection, climate sensitivity, and the tropical temperature response to warming.
7 While surface saturation specific humidity increases monotonically with temperature following the
8 Clausius-Clapeyron relation, moist-adiabatic warming varies non-monotonically with initial sur-
9 face temperature. Here, we explain the physical mechanism of this non-monotonicity. It emerges
10 from a competition between two limiting factors on the condensation rate of rising air: the avail-
11 ability of water vapor and adiabatic cooling. At low temperatures, condensation is limited by water
12 vapor and warming increases with initial surface temperature. At high temperatures, condensation
13 is limited by adiabatic cooling, which is increasingly offset by the latent heat released from conden-
14 sation. In other words, the moist enthalpy response to warming transitions from being dominated
15 by an increase in sensible enthalpy (warming) to an increase in latent enthalpy (moistening). The
16 criterion where this transition occurs is $L_v \partial_T q^* = c_{pd}$, i.e. where the temperature sensitivity of
17 latent enthalpy equals that of sensible enthalpy. We show this non-monotonicity propagates to buoy-
18 ancy and updraft velocity using a zero-buoyancy plume model. The non-monotonicity in updraft
19 velocity predicted by the theory is qualitatively consistent with that simulated by cloud-resolving
20 models.

21 **1. Introduction**

22 The Clausius-Clapeyron relation implies the potential for a warmer atmosphere to hold more
23 water vapor (Emanuel 1994). This principle is the basis for the positive water vapor feedback (Held
24 and Soden 2000). It also underpins various scaling theories for climate responses to warming,
25 including extreme precipitation, the Hadley cell edge, jet stream position, tropopause height, and
26 convective available potential energy (CAPE; O’Gorman 2015; Shaw and Voigt 2016; Romps
27 2016).

28 In the tropics, convection couples the surface to the free troposphere. Radiative cooling, which
29 acts to destabilize the atmosphere to convection, acts on slower timescales (order of days) compared
30 to convection (order of hours). As a result, the tropical atmosphere is to first order in a state of
31 quasi-equilibrium where the climatological free-tropospheric temperature follows a convectively
32 neutral profile set by the surface temperature and humidity Arakawa and Schubert (1974). Although
33 processes like convective entrainment influence the details of this coupling (Miyawaki et al. 2020;
34 Keil et al. 2021), moist-adiabatic adjustment is a useful first-order approximation (Held 1993). The
35 top-heavy warming profile predicted by moist-adiabatic adjustment (Fig. 1b) is a robust feature
36 in climate models and observations, despite historical challenges in observational records (Vallis
37 et al. 2015; Santer et al. 2005).

38 The top-heavy warming profile predicted by the moist adiabat is important because it increases
39 dry static stability. Spatial variations in dry static stability influence the structure of tropical
40 convergence zones because horizontal free-tropospheric gradients, while weak, exist (Neelin and
41 Held 1987; Bao et al. 2022). This structure also defines the tropical lapse rate feedback, a key
42 negative feedback for global climate sensitivity (Hansen et al. 1984). The lapse rate feedback
43 partially cancels the water vapor feedback and scales in tandem because amplified warming in
44 the upper troposphere is a consequence of increased surface water vapor and latent heat release
45 (Held and Shell 2012). In a moist-adiabatic atmosphere that is saturated at the surface, total latent
46 heat release is $L_v(q_s^* - q_{\text{top}}^*)$ where L_v is the latent heat of vaporization, q_s^* is surface saturation
47 specific humidity, and q_{top}^* is the cloud top saturation specific humidity. $q_{\text{top}}^* \rightarrow 0$ as $T \rightarrow 0$ in
48 a moist-adiabatic atmosphere because the moist adiabat does not predict a stratosphere¹. Thus

¹A more accurate proxy would consider how q_{top}^* varies with T_s . Assuming a fixed tropopause temperature = 200 K, q_{top}^* scales faster than Clausius-Clapeyron because of decreasing cloud top pressure with warming (Romps 2016).

49 we expect total latent heat release in a moist-adiabatic atmosphere to scale as q_s^* , which increases
 50 monotonically with surface temperature as expected from the Clausius-Clapeyron relation (Fig. 1a).

51 Given the monotonic increase in surface specific humidity with temperature, one might expect
 52 moist-adiabatic warming to also increase monotonically with the initial surface temperature at
 53 all levels. However, moist-adiabatic warming is a non-monotonic function of initial surface
 54 temperature (Fig. 1c, see Appendix A for details on calculating the moist adiabat). The non-
 55 monotonicity emerges in height coordinates (Fig. A1), with or without latent heat of fusion (see
 56 Appendix B and Fig. B1), and across different empirical formula for saturation vapor pressure
 57 (see Appendix C and Fig. C1). While previous work has acknowledged the existence of this
 58 non-monotonicity (Byrne and O’Gorman 2013; Levine and Boos 2016), an explanation does not
 59 yet exist in the literature.

60 This raises the question: what physical mechanism drives the non-monotonicity of moist-
 61 adiabatic warming? Here we explain the origin of the non-monotonicity in moist-adiabatic warming
 62 and its cascading effects on buoyancy and vertical velocity.

63 2. Theory of Non-Monotonic Warming

64 We start by defining the moist-adiabatic temperature profile in pressure coordinates $T(p)$ in
 65 terms of the moist-adiabatic lapse rate $\Gamma_m = dT/dp$:

$$66 T(p) = T_s + \int_{p_s}^p \Gamma_m dp' \quad (1)$$

72 where T_s is surface temperature. We assume the atmosphere is saturated from the surface. The
 73 difference between a perturbed and baseline state (Δ) then follows as

$$74 \Delta T(p) = \Delta T_s + \int_{p_s}^p \Delta \Gamma_m dp' \quad (2)$$

75 For a small perturbation, $\Delta \Gamma_m$ can be approximated using a first-order Taylor expansion: $\Delta \Gamma_m \approx$
 $\frac{d\Gamma_m}{dT_s} \Delta T_s$. Substituting this into Eq. (2) gives

$$76 \Delta T(p) \approx \Delta T_s + \left(\int_{p_s}^p \frac{d\Gamma_m}{dT_s} dp' \right) \Delta T_s \quad (3)$$

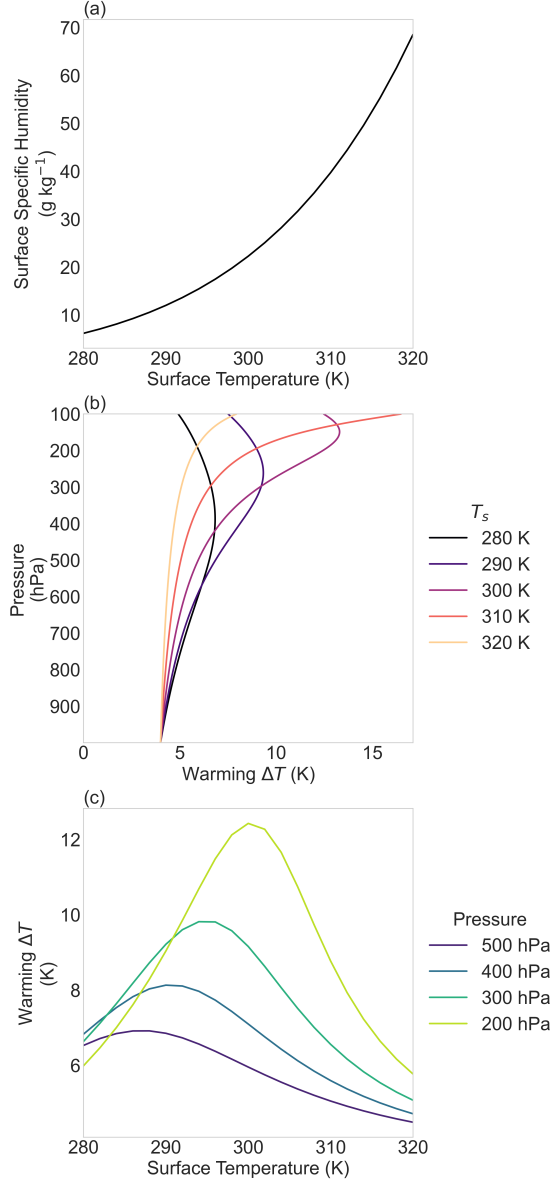


FIG. 1. (a) Surface saturation specific humidity increases monotonically with surface temperature. (b) Vertical profiles of moist-adiabatic warming to a 4 K surface warming for $T_s = 280, 290, 300, 310$, and 320 K. Warming decreases with initial surface temperature at lower levels while it increases with initial surface temperature at higher levels. (c) moist-adiabatic warming varies non-monotonically with initial surface temperature at all levels, e.g. at 500, 400, 300, and 200 hPa. moist-adiabatic warming peaks at warmer initial surface temperatures at higher levels.

The non-monotonicity in moist-adiabatic warming is encoded into $d\Gamma_m/dT_s$, the sensitivity of the moist-adiabatic lapse rate to surface temperature. Indeed, $d\Gamma_m/dT_s$ is non-monotonic with respect

78 to temperature, with a local minimum that varies as a function of surface temperature and pressure
 79 (dashed line in Fig. 2a). $d\Gamma_m/dT_s$ is mostly negative in the troposphere (Fig. 2b). This is consistent
 80 with amplified warming aloft because the integral in Eq. (2) is from high to low pressure, which
 81 introduces a negative sign.

82 Γ_m is a function of local temperature and pressure $\Gamma_m(T, p)$. To understand $d\Gamma_m/dT_s$, we rewrite
 83 it in terms of local state variables (T, p) using the chain rule:

$$\frac{d\Gamma_m}{dT_s} = \left(\frac{\partial \Gamma_m}{\partial T} \right)_p \cdot \frac{dT}{dT_s} + \left(\frac{\partial \Gamma_m}{\partial p} \right)_T \cdot \frac{dp}{dT_s} \quad (4)$$

84 The second term $\frac{dp}{dT_s} = 0$ because pressure, being the vertical coordinate, is independent of surface
 85 temperature. By definition $\Gamma_m = \frac{dT}{dp}$, so

$$\frac{d}{dp} \left(\frac{dT}{dT_s} \right) = \left(\frac{\partial \Gamma_m}{\partial T} \right)_p \cdot \frac{dT}{dT_s} \quad (5)$$

86 This is an ordinary differential equation for $\frac{dT}{dT_s}$ as a function of pressure. The solution with the
 87 boundary condition $\frac{dT}{dT_s}(p_s) = 1$, is

$$\frac{dT}{dT_s} = \exp \left(\int_{p_s}^p \left(\frac{\partial \Gamma_m}{\partial T} \right)_p dp' \right) \quad (6)$$

88 Substituting Eq. (6) into Eq. (4) gives

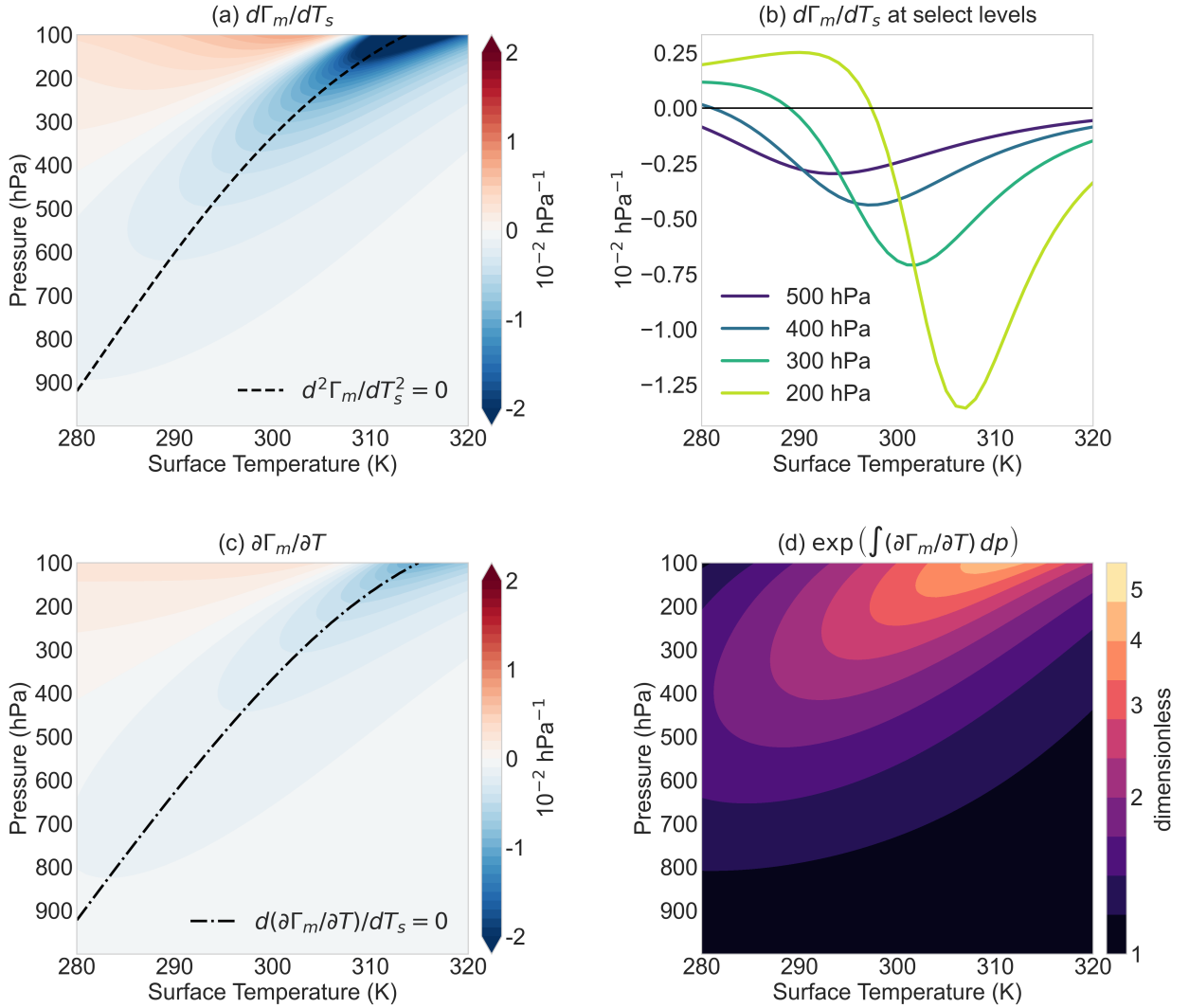
$$\frac{d\Gamma_m}{dT_s} = \left(\frac{\partial \Gamma_m}{\partial T} \right)_p \cdot \exp \left(\int_{p_s}^p \left(\frac{\partial \Gamma_m}{\partial T} \right)_{p'} dp' \right) \quad (7)$$

89 where $(\partial \Gamma_m / \partial T)_p$ is the moist-adiabatic lapse rate sensitivity to local temperature T at pressure
 90 level p . The integral describes how a small surface temperature perturbation dT_s influences
 91 $\Gamma_m(T, p)$ through the sum of all Γ_m changes that occur below pressure level p .

92 The non-monotonicity can emerge from

- 93 1. $\partial \Gamma_m / \partial T$ being non-monotonic and the integral acting to amplify it, or
 94 2. $\partial \Gamma_m / \partial T$ being monotonic but sign changes in $\partial \Gamma_m / \partial T$ leads to the integral being non-
 95 monotonic.

96 Numerical solutions show that $\partial\Gamma_m/\partial T$ is non-monotonic, with a local minimum that varies as a
 97 function of surface temperature and pressure (dash-dot line, $\partial\Gamma_m/\partial T$ in Fig. 2c). The integral term
 98 amplifies this non-monotonicity (Fig. 2d).



99 FIG. 2. (a) The sensitivity of the moist-adiabatic lapse rate, $d\Gamma_m/dT_s$, varies non-
 100 monotonically with surface temperature. (b) The local minimum of $d\Gamma_m/dT_s$ shifts toward warmer temperatures
 101 with surface temperature at higher levels. (c) The sensitivity of the moist-adiabatic lapse rate to the local
 102 temperature at pressure p , $\partial\Gamma_m/\partial T$, also varies non-monotonically with surface temperature. (d) The integral
 103 term in Eq. (7) amplifies the non-monotonicity of $\partial\Gamma_m/\partial T$. The surface temperature sensitivity of Γ_m (a) is the
 104 product of the local temperature sensitivity (c) and its integral (d), see Eq. (7).

¹⁰⁵ Why is $\partial\Gamma_m/\partial T$ non-monotonic? To understand this we solve for Γ_m from the first law of
¹⁰⁶ thermodynamics for adiabatic, non-precipitating, and reversible ascent of a saturated air parcel:

$$c_p dT - \alpha dp + L_v dq^* = 0 \quad (8)$$

¹⁰⁷ where c_p is the specific heat capacity of air at constant pressure, α is specific volume, L_v is the
¹⁰⁸ latent heat of vaporization, and q^* is the saturation specific humidity. We assume

- ¹⁰⁹ 1. $c_p \approx c_{pd}$, neglecting the role of water of all phases on the specific heat capacity, and
- ¹¹⁰ 2. $\alpha \approx \alpha_d = R_d T / p$, neglecting the virtual effect of water vapor on density.

¹¹¹ Next we use the chain rule to expand dq^* :

$$dq^* = \left(\frac{\partial q^*}{\partial T} \right)_p dT + \left(\frac{\partial q^*}{\partial p} \right)_T dp \quad (9)$$

¹¹² Substituting Eq. (9) into Eq. (8) and rearranging gives

$$\left(c_{pd} + L_v \left(\frac{\partial q^*}{\partial T} \right)_p \right) dT = \left(\alpha_d - L_v \left(\frac{\partial q^*}{\partial p} \right)_T \right) dp \quad (10)$$

¹¹³ We can derive closed-form expressions for the q^* derivatives using the Clausius-Clapeyron relation
¹¹⁴ and Dalton's Law. These q^* derivatives describe the role of phase equilibrium shifts in q^* with T
¹¹⁵ and p on the effective heat capacity and specific volume of the air parcel, respectively:

$$c_L \equiv L_v \left(\frac{\partial q^*}{\partial T} \right)_p \approx \frac{L_v^2 q^*}{R_v T^2} \quad (11)$$

$$\alpha_L \equiv -L_v \left(\frac{\partial q^*}{\partial p} \right)_T \approx \frac{L_v q^*}{p} \quad (12)$$

¹¹⁶ where the approximation comes from assuming that saturation vapor pressure $e^* \ll p$.

¹¹⁷ We interpret c_L as a latent heat capacity, which represents the increase in thermal inertia as latent
¹¹⁸ heating cancels part of the cooling from expansion. c_L acts to increase the heat capacity of the air
¹¹⁹ parcel such that it has an effective heat capacity $c_{pd} + c_L$.

120 We interpret α_L as a latent specific volume, which represents the enhanced expansion of air with
121 ascent as lower pressure shifts the phase equilibrium of water toward the vapor phase. α_L acts to
122 increase the volume of air such that it has an effective specific volume $\alpha_d + \alpha_L$.

123 Solving for the moist-adiabatic lapse rate $\Gamma_m = dT/dp$:

$$\Gamma_m = \frac{dT}{dp} = \frac{\alpha_d + \alpha_L}{c_{pd} + c_L} \quad (13)$$

$$= \Gamma_d \cdot \frac{1 + \frac{\alpha_L}{\alpha_d}}{1 + \frac{c_L}{c_{pd}}} \quad (14)$$

124 where $\Gamma_d = \alpha_d/c_{pd}$ is the dry adiabatic lapse rate in pressure coordinates and the two non-
125 dimensional terms represent the fractional increase in effective specific heat capacity and specific
126 volume due to the pressure and temperature sensitivities of the phase equilibrium of water:

$$\tilde{c} = \frac{c_L}{c_{pd}} = \frac{L_v^2 q^*}{c_{pd} R_v T^2} \quad (15)$$

$$\tilde{\alpha} = \frac{\alpha_L}{\alpha_d} = \frac{L_v q^*}{R_d T} = \frac{R_v c_{pd} T}{R_d L_v} \tilde{c} = k \tilde{c} \quad (16)$$

127 Substituting Eq. (15) and Eq. (16) into Eq. (14) gives

$$\Gamma_m = \Gamma_d \cdot \frac{1 + k \tilde{c}}{1 + \tilde{c}} \quad (17)$$

128 For typical values in Earth's atmosphere ($R_v = 461 \text{ J kg}^{-1} \text{ K}^{-1}$, $R_d = 287 \text{ J kg}^{-1} \text{ K}^{-1}$, $c_{pd} =$
129 $1005 \text{ J kg}^{-1} \text{ K}^{-1}$, $L_v = 2.5 \times 10^6 \text{ J kg}^{-1}$, and $T \in [200, 320] \text{ K}$), the factor $k = \frac{R_v c_{pd} T}{R_d L_v} \in [0.13, 0.21]$.
130 k is a weak function of temperature and is a quasi-constant of order 10^{-1} . In contrast, \tilde{c} scales
131 exponentially with temperature (through q^*) and varies from $\tilde{c}(200 \text{ K}) \sim 10^{-4}$ to $\tilde{c}(320 \text{ K}) \sim 10^1$.
132 The temperature sensitivity of Γ_m is controlled by \tilde{c} . In the dry limit $\tilde{c} \rightarrow 0$, $\Gamma_m \rightarrow \Gamma_d$. In the moist
133 limit $\tilde{c} \rightarrow \infty$, $\Gamma_m \rightarrow k \Gamma_d \sim 0.1 \Gamma_d$, so the moist adiabat cools slowly with height². Because Γ_m is
134 bounded, the magnitude of $\partial \Gamma_m / \partial T$ must peak at some intermediate \tilde{c} .

²This breaks down because the assumption $e^* \ll p$ is poor in a steam atmosphere where water vapor becomes a significant fraction of the atmosphere's mass, i.e. saturation mixing ratio $r^* \gtrsim 1$. At surface pressure this corresponds to $T \gtrapprox 360 \text{ K}$.

¹³⁵ Where does the magnitude of $\partial\Gamma_m/\partial T$ reach its peak value? To solve this we use the quotient
¹³⁶ rule on Eq. (13):

$$\frac{\partial\Gamma_m}{\partial T} = \underbrace{\frac{1}{c_{pd} + c_L} \frac{\partial(\alpha_d + \alpha_L)}{\partial T}}_{\text{latent volume sensitivity}} + \underbrace{\left(-\frac{\alpha_d + \alpha_L}{(c_{pd} + c_L)^2} \frac{\partial c_L}{\partial T} \right)}_{\text{latent heat capacity sensitivity}} \quad (18)$$

¹³⁷ The latent volume sensitivity varies monotonically with surface temperature (Fig. 3a, c). The
¹³⁸ non-monotonicity is due to the latent heat capacity sensitivity (Fig. 3b, d) so we further decompose
¹³⁹ it to identify its origin:

$$-\frac{\alpha_d + \alpha_L}{(c_{pd} + c_L)^2} \frac{\partial c_L}{\partial T} = -\frac{1}{p} \cdot (1 + \tilde{\alpha}) \cdot \frac{R_d}{c_{pd}} \frac{\partial \log c_L}{\partial \log T} \cdot f_d \cdot f_L \quad (19)$$

¹⁴⁰ where

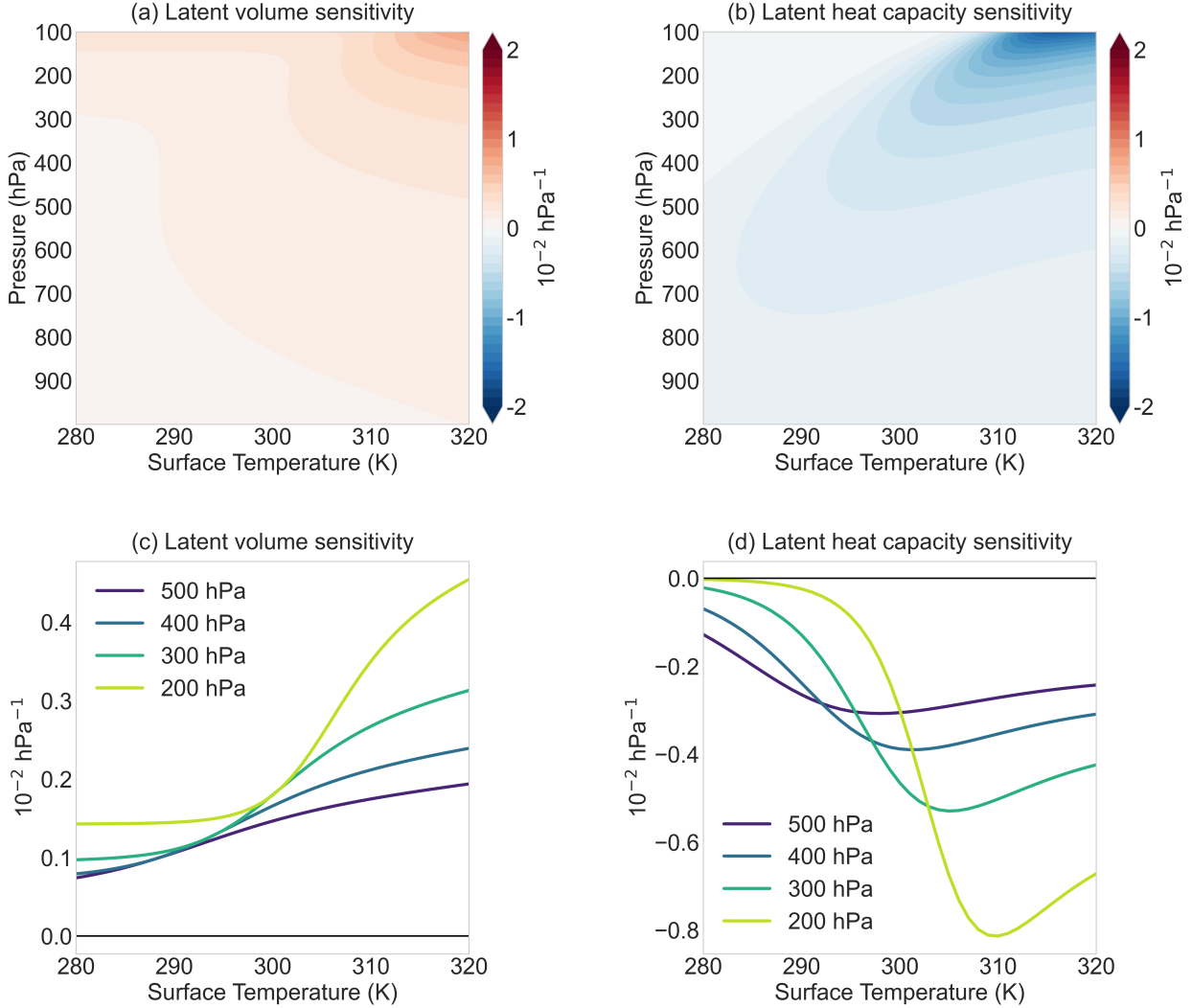
$$f_d \equiv c_{pd}/(c_{pd} + c_L) \quad (20)$$

$$f_L \equiv c_L/(c_{pd} + c_L) \quad (21)$$

¹⁴² and $f_d + f_L = 1$. f_d and f_L represent the sensible and latent fractions of effective heat capacity,
¹⁴³ respectively. f_d quantifies the fraction of the moist enthalpy change associated with an increase
¹⁴⁴ in sensible enthalpy (i.e. warming) while f_L quantifies the fraction associated with an increase in
¹⁴⁵ latent enthalpy (i.e. moistening).

¹⁵¹ Eq. (19) shows the latent heat capacity sensitivity is a product of four terms that vary mono-
¹⁵² tonically with T . $\tilde{\alpha} = L_v q^*/(\alpha_d p)$ scales exponentially with T through q^* (dashed line in
¹⁵³ Fig. 4a). The fractional change in latent heat capacity to a fractional change in temperature
¹⁵⁴ $\partial \log c_L / \partial \log T = L_v / (R_v T) - 2$ decreases with T (dotted line in Fig. 4a). The product of these
¹⁵⁵ two terms is weakly non-monotonic in T with a local minimum located approximately where
¹⁵⁶ $\tilde{\alpha} = R_v T / L_v$ (white line in Fig. 4b). At low T , $\tilde{\alpha}$ is small so the product is dominated by the
¹⁵⁷ decrease in $\partial \log c_L / \partial \log T$. At high T , $\tilde{\alpha}$ is large so the product is dominated by the exponential
¹⁵⁸ increase in $\tilde{\alpha}$. However, the non-monotonicity that emerges from these two terms is not the source
¹⁵⁹ of the peak magnitude in $\partial\Gamma_m/\partial T$, which requires a local maximum, not a minimum.

¹⁶⁰ The sensible fraction of effective heat capacity f_d logically decreases with T because c_{pd} is
¹⁶¹ a constant while latent heat capacity c_L increases exponentially with T through q^* (red line in



146 FIG. 3. The moist-adiabatic lapse rate sensitivity to local temperature T , $\partial\Gamma_m/\partial T$ (Fig. 2c), is decomposed into
 147 contributions from (a) the latent volume sensitivity and (b) the latent heat capacity sensitivity following Eq. (18).
 148 (c) The latent volume sensitivity monotonically increases with local temperature T across all pressure
 149 levels, e.g. across 500, 400, 300, and 200 hPa. (d) The latent heat capacity sensitivity has a local minimum that
 150 shifts toward warmer surface temperature at higher levels, consistent with the behavior of $d\Gamma_m/dT_s$ (Fig. 2b).

162 Fig. 4c). The latent fraction of effective heat capacity f_L logically increases with T (blue line in
 163 Fig. 4c). The product $f_d \cdot f_L$ peaks when $f_d = f_L$, or $c_L = c_{pd}$ (black line in Fig. 4d).

164 What is the physical intuition behind the peak occurring at $c_L = c_{pd}$? Recall that c_L quantifies the
 165 enhancement of effective heat capacity due to condensation heating offsetting adiabatic cooling.
 166 Condensation ($\partial_T q^*$ in c_L) requires two ingredients: 1) cooling from expansion and 2) water vapor.

f_d and *f_L* correspond to the fractional availability of the two ingredients. At low *T* (*c_{L < *c_{pd}*), condensation is limited by the availability of water vapor (blue line in Fig. 4c). The moist enthalpy response to warming is dominated by an increase in sensible enthalpy (warming). At high *T* (*c_{L > *c_{pd}*), condensation is limited by adiabatic cooling (red line in Fig. 4c), which means the rising parcel retains more water as vapor instead of condensation. The moist enthalpy response to warming is dominated by an increase in latent enthalpy (moistening). The peak in latent heat capacity sensitivity corresponds to where the availability of water vapor and cooling are equally limiting (black line in Fig. 4c). The non-monotonicity in $\partial\Gamma_m/\partial T$ and moist-adiabatic warming emerges from the competition between the two limiting factors of condensation, which controls the partitioning of the moist enthalpy response to warming into sensible and latent enthalpy.}*}*

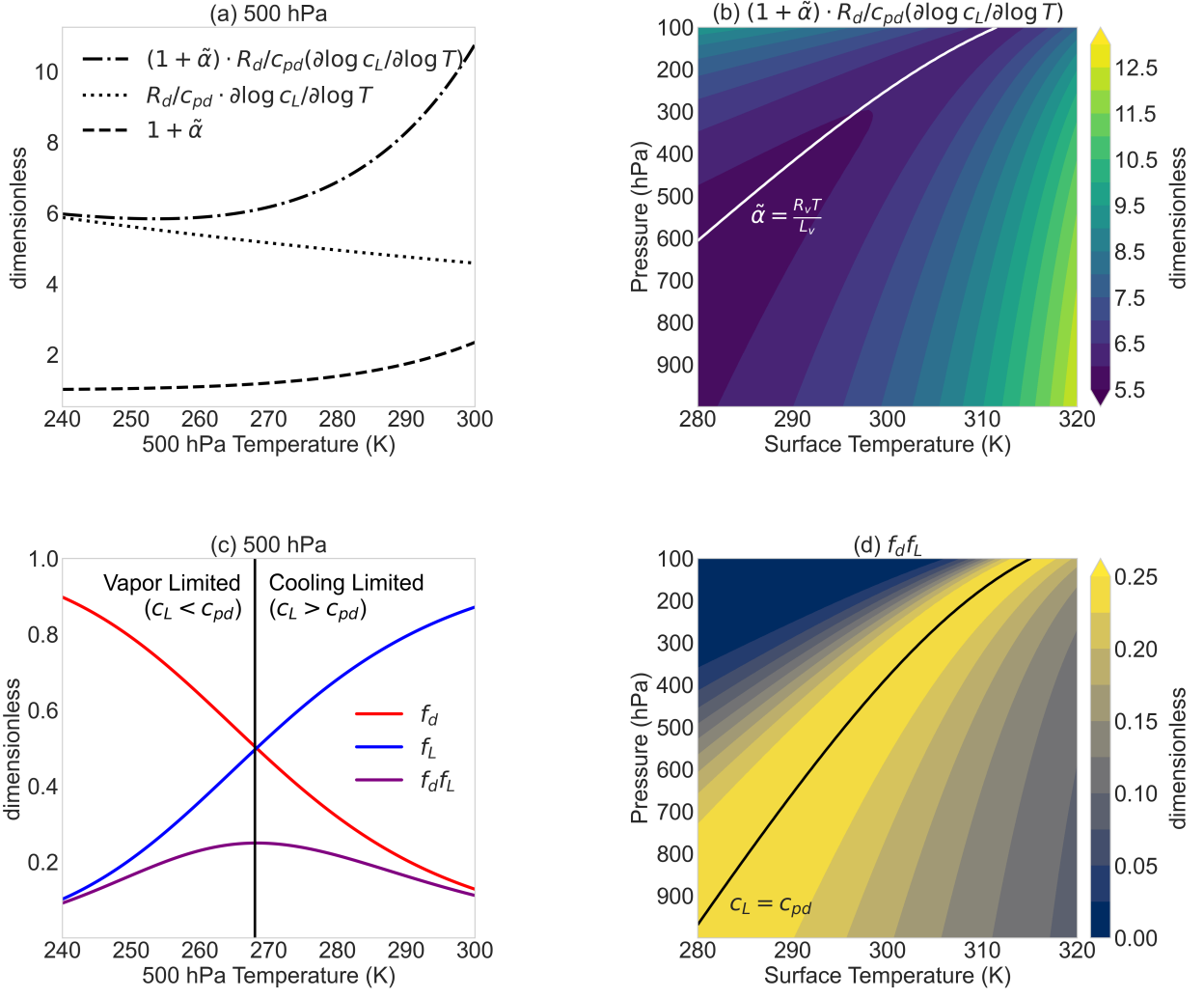
How well does the condition *c_{L = *c_{pd}* capture the actual peak in $\partial\Gamma_m/\partial T$? The theory overpredicts the *T_s* where the magnitude of $\partial\Gamma_m/\partial T$ peaks (compare solid and dash-dot lines in Fig. 5). This error is due to the weak non-monotonicity in the product $(1 + \tilde{\alpha})R_d/c_{pd}\partial\log(c_L)/\partial\log(T)$ which decreases with height (Fig. 4b). The error maximizes at the surface where the theory predicts a peak *T_s* that is 1.6 K warmer than the true peak *T_s*.}*

The difference in *T_s* predicted by the theory and the true peak of Γ_m/dT_s grows with height because the integral term in Eq. (7) amplifies the error in $\partial\Gamma_m/\partial T$ at each level below. This error maximizes at 420 hPa where *c_{L = *c_{pd}* predicts a peak *T_s* that is 2.0 K warmer than the true peak *T_s* (compare solid and dashed lines in Fig. 5). This error compounds for *T_s* of peak moist-adiabatic warming ΔT (Eq. 3), leading to a maximum error of 6.6 K at 382 hPa (compare solid and dotted lines in Fig. 5). Thus the condition *c_{L = *c_{pd}* is a useful first-order estimate of the *T_s* where moist-adiabatic warming peaks.}*}*

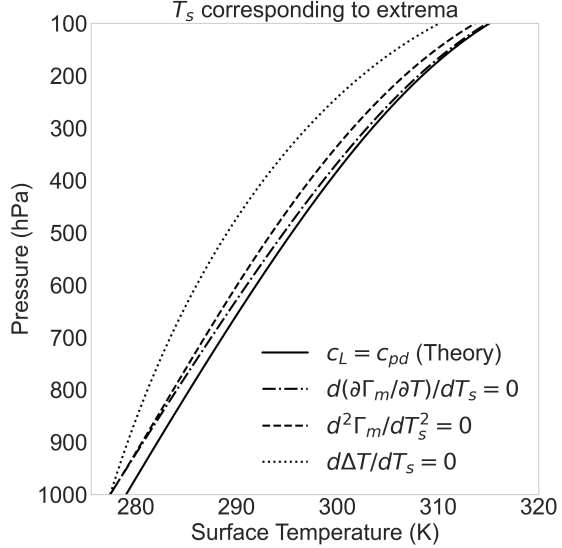
3. Implications for Convective Dynamics

The non-monotonicity of moist-adiabatic warming has implications for convective dynamics. For example, Romps (2016) showed that parcel buoyancy is a non-monotonic function of surface temperature. Specifically the criterion where *B* peaks is $\beta = 2c_{pd}$ where

$$\beta = c_{pd} + L_v \frac{\partial q^*}{\partial T} = c_{pd} + c_L \quad (22)$$



177 FIG. 4. The latent heat capacity sensitivity is decomposed into a product of four terms (Eq. 19) that vary
 178 monotonically with local temperature T , where local means at pressure p . (a) The latent volume ratio $\tilde{\alpha}$ increases
 179 exponentially with T (dashed) while the fractional change in latent heat capacity c_L to a fractional change in T
 180 decreases approximately linearly with T (dotted). The product of the two is weakly non-monotonic with T where
 181 the product has a local minimum (dash-dot). (b) The local minimum across the pressure-surface temperature
 182 space approximately occurs where $\tilde{\alpha} = R_v T / L_v$ (white line). (c) The latent fraction of effective heat capacity
 183 f_L increases logarithmically with T (blue line) while the sensible fraction f_d decreases logarithmically with T . (d)
 184 The product of the two is non-monotonic with T where the product has a local maximum (purple line). (d) The
 185 $f_d \cdot f_L$ local maximum across the pressure-surface temperature space occurs where $c_L = c_{pd}$ (black line).



198 FIG. 5. Surface temperature T_s corresponding to the criterion $c_L = c_{pd}$ (solid), the minimum of the moist-
 199 adiabatic lapse rate sensitivity to local temperature $\partial\Gamma_m/\partial T$ (dash dot), the minimum of the moist-adiabatic
 200 lapse rate sensitivity to surface temperature $d\Gamma_m/dT_s$ (dashed), and the maximum of moist-adiabatic warming
 201 ΔT (dotted). The theory most accurately captures the T_s corresponding to the minimum of $\partial\Gamma_m/\partial T$. The
 202 discrepancy between the theory and the T_s corresponding to the minimum of $d\Gamma_m/dT_s$ and ΔT is larger because
 203 the error at pressure p is the accumulation of errors at levels below p (see Eq. 7 and 3).

208 Thus the Romps (2016) criterion that maximizes B is equivalent to the criterion where moist-
 209 adiabatic warming peaks, $c_L = c_{pd}$. We show this is true if the entrainment parameter a is small
 210 and derive a more general criterion that maximizes buoyancy.

211 Buoyancy B is the normalized virtual temperature (or equivalently, density) difference between
 212 the rising parcel $T_{v,p}$ and the environment $T_{v,e}$. Here we neglect the virtual effects of water and use
 213 standard temperature:

$$B \approx \frac{g}{T_e} (T_p - T_e) \quad (23)$$

214 As before, we express temperature profiles in terms of T_s and the integral of their respective lapse
 215 rates. We assume the parcel follows a moist-adiabatic lapse rate, Γ_m , while the environment is
 216 neutrally buoyant with respect to an entraining lapse rate, Γ_e , following the zero-buoyancy plume

²¹⁷ model (Singh and O’Gorman 2013):

$$T_p = T_s + \int_{p_s}^p \Gamma_m(p') dp' \quad (24)$$

$$T_e = T_s + \int_{p_s}^p \Gamma_e(p') dp' \quad (25)$$

²¹⁸ Substituting Eq. (24) and (25) into the definition of buoyancy Eq. (23) yields

$$B \approx \frac{g}{T_e} \int_{p_s}^p \delta\Gamma dp' \quad (26)$$

²¹⁹ where $\delta\Gamma = \Gamma_e - \Gamma_m$. We use the entraining lapse rate Γ_e as in Romps (2016) but expressed in
²²⁰ pressure coordinates:

$$\Gamma_e = \Gamma_d \cdot \frac{(1+a)\alpha_d + \alpha_L}{(1+a)c_{pd} + c_L} \quad (27)$$

²²¹ Substituting Eq. (13) and Eq. (27) into Eq. (26) and simplifying gives

$$B = \frac{g}{T_e} \int_{p_s}^p \Gamma_d \cdot \frac{a(1-k)\tilde{c}}{(1+a+\tilde{c})(1+\tilde{c})} dp' \quad (28)$$

²²² Under the simplifying assumption that entrainment parameter a is constant with T_s , T_e increases
²²³ monotonically with T_s at all p . Then the origin of the non-monotonicity of B must be in the
²²⁴ integrand, $\delta\Gamma$. B depends on T primarily through \tilde{c} , which scales exponentially with T through
²²⁵ q^* , whereas Γ_d and k are linear functions of T . In the limit of $\tilde{c} \rightarrow 0$ (cold and dry), $\delta\Gamma$ scales
²²⁶ as \tilde{c} , which increases with T . In the limit of $\tilde{c} \rightarrow \infty$ (warm and humid), $\delta\Gamma$ scales as \tilde{c}^{-1} , which
²²⁷ decreases with increasing T . This means $\delta\Gamma$ maximizes at some intermediate \tilde{c} .

²²⁸ To solve for the condition that maximizes buoyancy we solve for the \tilde{c} derivative of the integrand
²²⁹ $\delta\Gamma$ in Eq. (28) and set it to zero:

$$\frac{d}{d\tilde{c}} \left(\Gamma_d \cdot \frac{a(1-k)\tilde{c}}{(1+a+\tilde{c})(1+\tilde{c})} \right) = 0 \quad (29)$$

²³⁰ If we assume that a , k , and Γ_d do not vary with T , the solution to Eq. (29) is

$$\tilde{c}_{\text{peak}} = \sqrt{1+a} \quad (30)$$

231 Thus the condition that maximizes buoyancy is $c_L = \sqrt{1+a}c_{pd}$. In the limit of weak entrainment
 232 $a \rightarrow 0$, this reduces to $c_L = c_{pd}$. In the presence of entrainment, buoyancy peaks at a higher c_L and
 233 so higher T_s all else equal. Entrainment dilutes the air parcel and reduces the latent heat released
 234 by the cooling parcel given the same q^* . The factor $\sqrt{1+a}$ describes the shift in the critical
 235 point separating the vapor limited and cooling limited regimes toward higher q^* in the presence of
 236 entrainment.

237 How important is the factor $\sqrt{1+a}$? For an entrainment rate representative of Earth's current
 238 climate $a = 0.2$, the difference in T_s of $c_L = c_{pd}$ and $c_L = \sqrt{1+a}c_{pd}$ are < 1.49 K (compare red
 239 and solid black lines in Fig. 6a). This difference decreases with height and becomes insignificant
 240 around the tropopause (0.46 K at $p = 200$ hPa). This is why the criterion $c_L = c_{pd}$ works well for
 241 explaining the non-monotonicity of CAPE for present Earth-like climates (Romps 2016). However,
 242 for stronger entrainment rates and for understanding the non-monotonicity of buoyancy in the lower
 243 troposphere, the factor $\sqrt{1+a}$ becomes more important (e.g., 4.38 K for $a = 0.7$ at the surface;
 244 compare red and solid black lines in Fig. 6b).

245 How well do these criteria capture the T_s that maximizes buoyancy across the troposphere? We
 246 first focus on $\delta\Gamma$, i.e. the integrand in Eq. (26). For $a = 0.2$, both criteria capture the T_s of peak
 247 $\delta\Gamma$ well (< 1.39 K for $c_L = \sqrt{1+a}c_{pd}$, < 2.87 K for $c_L = c_{pd}$, compare red and solid black lines
 248 to dashed line in Fig. 6a). The small error arises even for the $c_L = \sqrt{1+a}c_{pd}$ criterion because
 249 $\Gamma_d(1-k)$ is weakly non-monotonic with T (Γ_d increases with T and $(1-k)$ decreases with T),
 250 which we ignored earlier in order to analytically solve Eq. (29). This error is amplified as we
 251 integrate $\delta\Gamma$ to obtain buoyancy Eq. (26) because the error in T_s of peak $\delta\Gamma$ from levels below p
 252 accumulates for the T_s of peak B (compare red and solid black lines to dotted line in Fig. 6a).

253 For a higher entrainment parameter $a = 0.7$ the importance of the factor $\sqrt{1+a}$ becomes clear.
 254 The error in T_s of peak $\delta\Gamma$ is < 3.39 K for the $c_L = \sqrt{1+a}c_{pd}$ criterion compared to < 5.83 K for
 255 the $c_L = c_{pd}$ criterion (compare red and solid black lines to dashed line in Fig. 6b). The error in T_s
 256 of peak buoyancy is lower for the $c_L = c_{pd}$ criterion (< 3.37 K) compared to the $c_L = \sqrt{1+a}c_{pd}$
 257 criterion (< 4.66 K, compare red and solid black lines to dotted black line in Fig. 6b). This is
 258 because $c_L = c_{pd}$ underpredicts T_s for peak B in the lower troposphere, which offsets the growth of
 259 the larger error in peak $\delta\Gamma$ (compare solid black and dotted lines in Fig. 6b). The criterion $c_L = c_{pd}$
 260 predicts the T_s of peak buoyancy better than $c_L = c_{pd}\sqrt{1+a}$ in some cases because of a cancellation

261 of errors rather than for the right physical reason. For example the criterion $c_L = c_{pd}$ predicts
 262 no shift in T_s that maximizes B to variations in a while the criterion $c_L = \sqrt{1+ac_{pd}}$ qualitatively
 263 captures the shift in peak $\delta\Gamma$ and B toward warmer T_s with increasing entrainment (Fig. 6c).

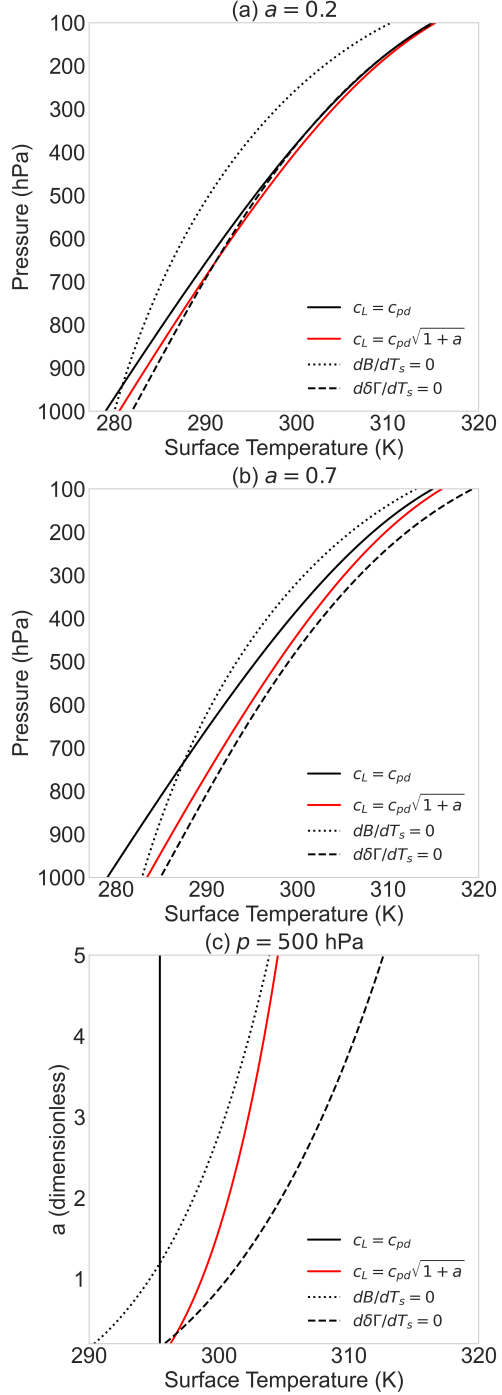
270 The non-monotonicity of buoyancy with surface temperature extends to the strength of the
 271 convective updraft. We model the updraft's specific kinetic energy, $\frac{1}{2}w^2$, using Eq. (1) from
 272 Del Genio et al. (2007):

$$\frac{d}{dz} \left(\frac{1}{2}w^2 \right) = a'B(z) - (1+b')\epsilon(z)w^2 \quad (31)$$

273 where a' and b' are dimensionless constants. We use $a' = 1/6$ and $b' = 2/3$ following Del Genio
 274 et al. (2007). We calculate the fractional entrainment rate $\epsilon(z)$ following Eq. (3) in Romps
 275 (2016) with entrainment parameter $a = 0.2$ and precipitation efficiency $PE = 0.35$. Since $w(z)$ is
 276 determined by the integral of the net force, which includes buoyancy, we expect updraft velocity
 277 to also vary non-monotonically with surface temperature.

278 Numerically integrating Eq. (31) confirms this expectation. Updraft velocity varies non-
 279 monotonically with T_s , updraft velocity decreases with surface temperature at lower levels while
 280 it increases with surface temperature at higher levels (Fig. 7a). The surface temperature of peak
 281 updraft velocity increases at higher levels, consistent with the non-monotonicity of moist-adiabatic
 282 warming and buoyancy (Fig. 7b).

283 Is this result relevant to Earth's atmosphere, where convective thermodynamics is not strictly
 284 moist-adiabatic and dynamics is subject to details and constraints not considered here such as
 285 cloud microphysics, radiative transfer, and turbulence? There are examples in the literature
 286 that show both buoyancy and updraft velocity diagnosed from cloud-resolving models vary non-
 287 monotonically with surface temperature. Buoyancy profiles simulated by Das Atmosphärische
 288 Modell and predicted by the zero-buoyancy plume model agree well across a large range of surface
 289 temperature (Fig. 2a in Seeley and Romps 2015). Updraft velocity profiles simulated by CM1 (Fig. 2
 290 in Singh and O'Gorman 2015) is qualitatively consistent with Eq. (31) but there are quantitative
 291 differences. CM1 simulates a decrease in updraft velocity with T_s below 900 hPa while Eq. (31)
 292 predicts a decrease in vertical velocity with T_s below a much deeper layer, $z \approx 11$ km at 300 K. To
 293 understand the applicability and robustness of the non-monotonicity in updraft velocity predicted
 294 by Eq. (31), we analyzed 9 cloud-resolving models simulating radiative convective equilibrium in a
 295 100 km x 100 km domain from the RCEMIP project (Wing et al. 2018). We define updraft velocity



264 FIG. 6. Surface temperature T_s corresponding to the criterion $c_L = c_{pd}$ (solid black), the criterion $c_L =$
 265 $c_{pd}\sqrt{1+a}$ (red), the maximum of buoyancy B (dotted), and the minimum of the difference between an entraining
 266 lapse rate and moist-adiabatic lapse rate $\delta\Gamma = \Gamma_e - \Gamma_m$ (dashed) for the entrainment parameter (a) $a = 0.2$ and (b)
 267 $a = 0.7$. (c) The criterion $c_L = c_{pd}\sqrt{1+a}$ captures the a dependence of $\delta\Gamma$ and B extrema evaluated at pressure
 268 $p = 500 \text{ hPa}$. In comparison the criterion $c_L = c_{pd}$ is not sensitive to the entrainment parameter a (vertical black
 269 line).

as the mean of vertical velocity w exceeding the 99.9th percentile ($w > 99.9$) at each height for w aggregated over horizontal space and the last 25 days of each simulation. The 99.9th percentile corresponds to the fastest 1000 samples of w per level per model run. We focus on the strongest convective updrafts because a moist-adiabatic profile is most relevant for the convective core of the strongest updrafts (Riehl and Malkus 1958).

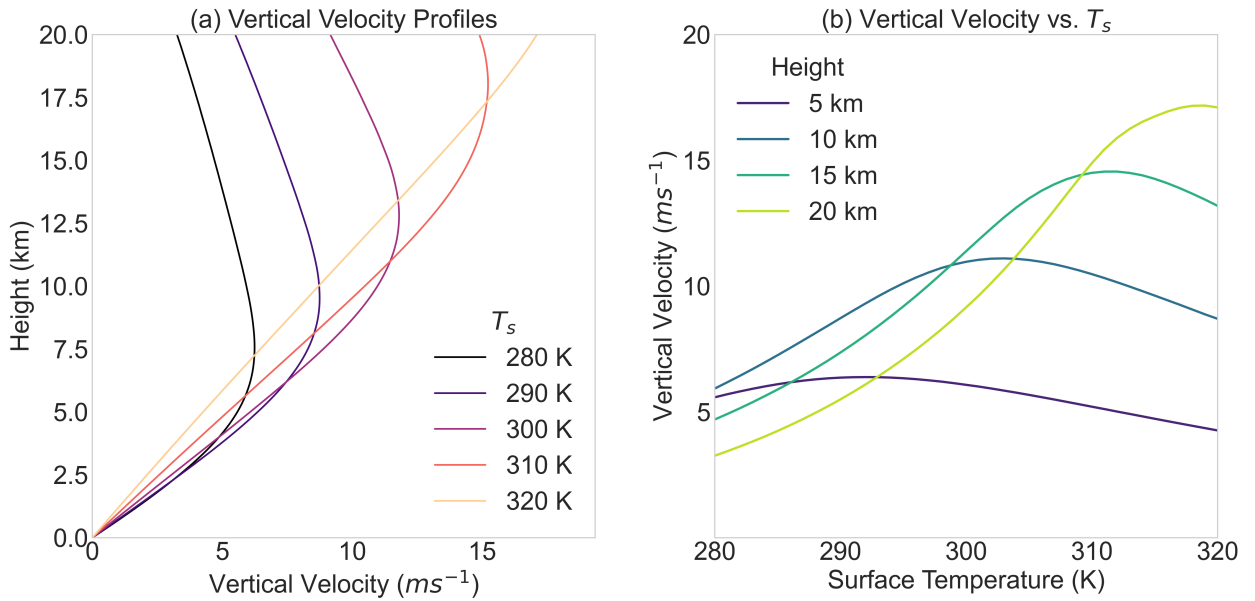


FIG. 7. (a) Vertical profiles of updraft velocity, calculated by numerically integrating Eq. (31) in height using buoyancy B from Eq. (23). Updraft velocity decreases with surface temperature at lower levels while it increases with surface temperature at higher levels. (b) Updraft velocity varies non-monotonically with surface temperature at all levels, e.g. at 5, 10, 15, and 20 km. Updraft velocity peaks at warmer surface temperatures at higher levels consistent with the behavior of buoyancy (Fig. 6a) and moist-adiabatic warming (Fig. 5).

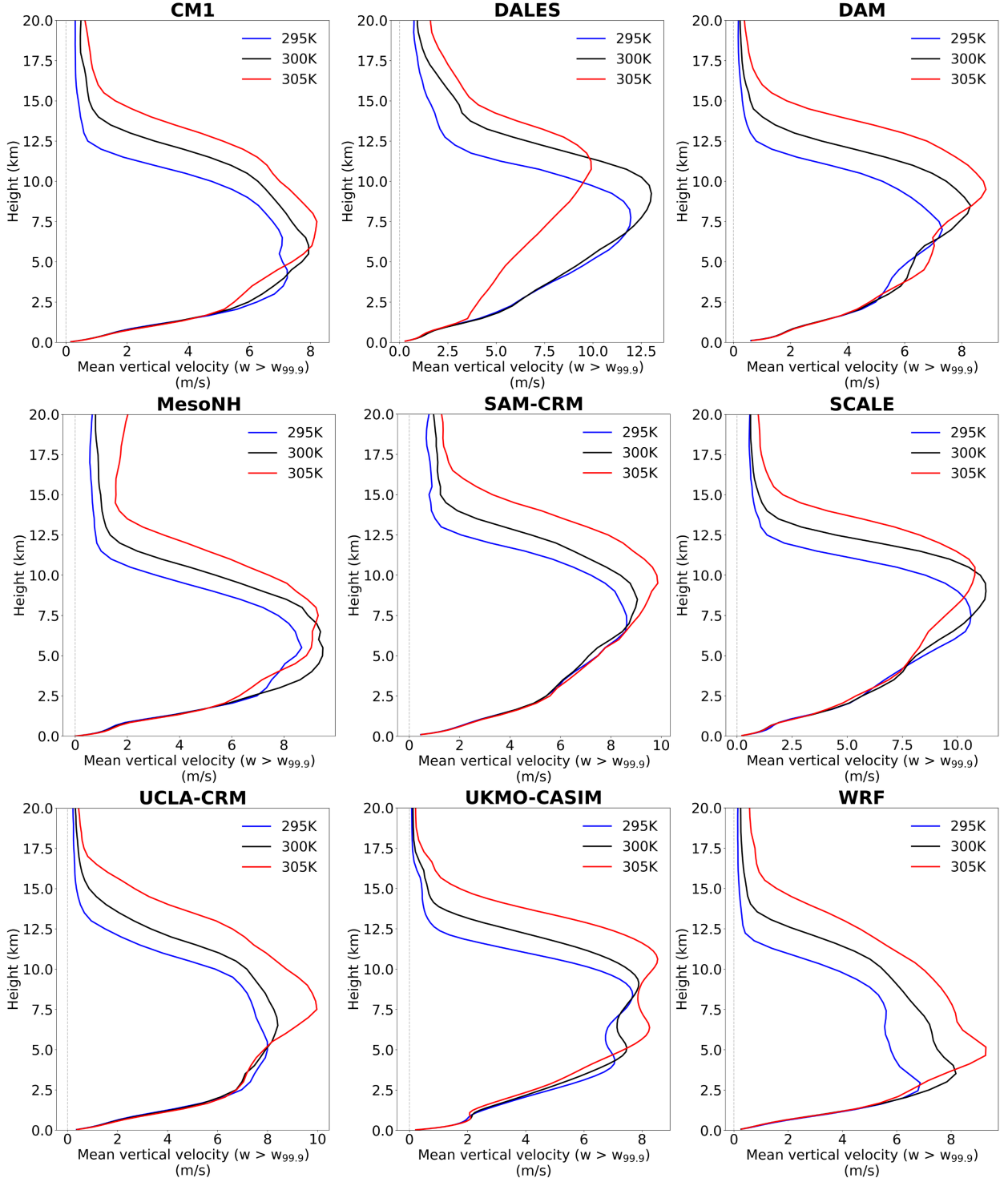
There is a large diversity of updraft velocity in the RCEMIP simulations to variations in surface temperature (295, 300, and 305 K, see Fig. 8). Some models exhibit a clear shift toward increasingly top-heavy updraft velocity profiles with warming (e.g., CM1, DAM, UCLA-CRM, UKMO, WRF). In these models, updraft velocity decreases at lower levels, which is qualitatively consistent with Eq. (31) (Fig. 7a). SAM shows a top-heavy shift in updraft velocity without a clear decrease in lower levels. In the remaining models updraft velocity is non-monotonic with T_s but the T_s of peak updraft velocity does not increase to higher levels as expected from Eq. (31) (Fig. 7b). For example DALES and SCALE predict a non-monotonic response in updraft velocity with T_s at $z \approx 8$ km but

the peak updraft velocity weakens from $T_s = 300$ to 305 K. MesoNH also predicts a decrease in peak updraft velocity from $T_s = 300$ K to 305 K but predicts a non-monotonic response in updraft velocity with T_s at $z \approx 3$ km, much lower than in DALES and SCALE. The diversity of updraft velocity profiles likely emerges from differences in model details such as parameterization schemes for cloud microphysics, radiative transfer, and turbulence in addition to emergent behavior such as convective organization. Nonetheless, the presence of non-monotonicity in all but one model suggests that the simple mechanism controlling non-monotonicity in moist-adiabatic warming may be playing a role in shaping the variation of updraft velocity profiles across surface temperature in models that explicitly resolve convective storms.

4. Summary and Discussion

moist-adiabatic warming varies non-monotonically with respect to initial surface temperature. The non-monotonicity occurs because of a competition between two limiting factors of condensation: availability of water vapor and adiabatic cooling. At low temperature, condensation is limited by the availability of water vapor and moist-adiabatic warming scales like Clausius-Clapeyron. At high temperature, condensation is limited by the diminishing net cooling with ascent because high latent heating cancels an increasingly larger fraction of adiabatic cooling. In other words, the moist enthalpy response to warming is dominated by an increase in sensible enthalpy at low temperature and an increase in latent enthalpy at high temperature. The repartitioning of the dominant term in the moist enthalpy response to warming ($c_L = c_{pd}$) corresponds to where moist-adiabatic warming peaks. The non-monotonicity of moist-adiabatic warming propagates to buoyancy as predicted by the zero-buoyancy plume model because the repartitioning of the moist enthalpy response from sensible to latent enthalpy with increasing temperature occurs in both entraining and moist-adiabatic lapse rates. The surface temperature where the buoyancy peaks follows $c_L = c_{pd}\sqrt{1+a}$, where a is the entrainment parameter as defined in Romps (2016). The non-monotonicity of buoyancy also propagates to updraft velocity. Cloud-resolving models simulating radiative-convective equilibrium exhibit diverse but qualitatively consistent responses of strong convective updrafts to surface temperature changes as predicted by the zero-buoyancy plume model.

The $c_L = c_{pd}$ criterion was first used to explain why buoyancy profiles are top heavy (Seeley and Romps 2016). Buoyancy maximizes where the saturation moist static energy difference between



323 FIG. 8. Updraft velocity from 9 cloud-resolving models (CM1, DALES, DAM, MesoNH, SAM-CRM, SCALE,
 324 UCLA-CRM, UKMO-CASIM, and WRF) that participated in RCEMIP (Wing et al. 2018). The simulations are
 325 on a $100 \text{ km} \times 100 \text{ km}$ periodic domain for uniform sea surface temperatures set to 295 (blue), 300 (black), and
 326 305 K (red). Updraft velocity at each level is the mean of vertical velocities w that exceed the 99.9th percentile
 327 ($w_{99.9}$, defined separately for each model).

348 the environment and parcel (δh^*) is expressed as a temperature difference (sensible enthalpy
 349 difference, $c_{pd}\delta T$) rather than a humidity difference (latent enthalpy difference, $L_v\delta q^*$). The ratio
 350 $\tilde{c} = c_L/c_{pd} = L_v\delta q^*/(c_{pd}\delta T)$ quantifies the transition where δh^* is expressed largely in terms of
 351 $L_v\delta q^*$ (lower troposphere, where $\tilde{c} > 1$) and in terms of $c_{pd}\delta T$ (upper troposphere, where $\tilde{c} < 1$).
 352 and Romps (2016) explained the non-monotonicity of buoyancy at the tropopause to explain the
 353 non-monotonicity of CAPE with surface temperature. Following the same reasoning as in Seeley
 354 and Romps (2016), Romps (2016) shows that tropopause buoyancy and CAPE peak where $c_L = c_{pd}$.
 355 We show that a more general criterion for the T_s of peak buoyancy is $c_L = c_{pd}\sqrt{1+a}$, which reduces
 356 to $c_L = c_{pd}$ in the limit of weak entrainment. The factor $\sqrt{1+a}$ is insignificant in Earth's current
 357 climate (e.g. for $a = 0.2$, $\sqrt{1+a} = 1.09$) so Romps (2016)'s criterion works well for understanding
 358 the non-monotonicity of CAPE on present Earth-like atmospheres. However, the factor $\sqrt{1+a}$
 359 is important for understanding the non-monotonicity of buoyancy at lower levels and CAPE in a
 360 world with stronger entrainment rates than on present Earth.

361 Curiously, the surface temperature of peak CAPE (≈ 335 K, Romps 2016) is similar to the
 362 surface temperature that marks the transition to a moist greenhouse regime (≈ 335 K, Komabayashi
 363 1967; Ingersoll 1969; Kasting 1988). Is this similarity due to a shared physical mechanism or
 364 a coincidence? The criterion for peak CAPE is $L_v(\partial_T q^*)|_t = c_{pd}$, i.e. the surface temperature
 365 where the *temperature sensitivity* of latent and sensible enthalpy at the *tropopause* are equal. On
 366 the other hand the criterion for the transition to a moist greenhouse is $L_v q_s^* = c_{pd}T_s$, i.e. the
 367 surface temperature where the *magnitude* of latent and sensible enthalpy at the *surface* are equal
 368 (Wordsworth and Pierrehumbert 2013). The ratio of the temperature sensitivity of latent and
 369 sensible enthalpy at the tropopause scales differently from the ratio of the magnitude of latent and
 370 sensible enthalpy at the surface (Fig. D1, see Appendix D for more detail). While these thresholds
 371 coincide around 335 K in Earth-like climates, their underlying scalings differ, suggesting that they
 372 may diverge in other planetary climates.

373 The non-monotonicity of moist-adiabatic warming may have additional implications for climate,
 374 such as the organization of convection and the large-scale circulation response to warming. For
 375 example, Shaw and Miyawaki (2025) explain the mechanism behind the $2\% \text{ K}^{-1}$ scaling of the mean
 376 and extreme upper-level wind response to warming by assuming a moist-adiabatic atmosphere.
 377 The non-monotonicity of moist-adiabatic warming would drive a non-monotonic change in the

378 meridional and zonal temperature gradients at fixed height and pressure levels. This could serve
379 as a thermodynamically driven hypothesis for the potential of non-monotonicities to emerge in
380 dynamical responses to warming such as in the response of jet stream wind, extratropical cyclones,
381 and mean overturning circulations.

382 *Acknowledgments.* I thank the Union College Faculty Research Fund and the NSF National Center
383 for Atmospheric Research Advanced Studies Program for supporting this work. I thank Andrew
384 Williams, Jiawei Bao, Jonah Bloch-Johnson, Martin Singh, Stephen Po-Chedley, Nadir Jeevanjee,
385 and two anonymous reviewers for helpful discussions and feedback on the manuscript.

386 *Data availability statement.* All scripts used for analysis and plots in this paper are available at
387 <https://github.com/omiyawaki/miyawaki-2025-nonmonotonic-moist-adiabat>. They
388 will also be archived on Zenodo upon publication.

389 APPENDIX A

390 **Calculating moist-adiabatic Profiles**

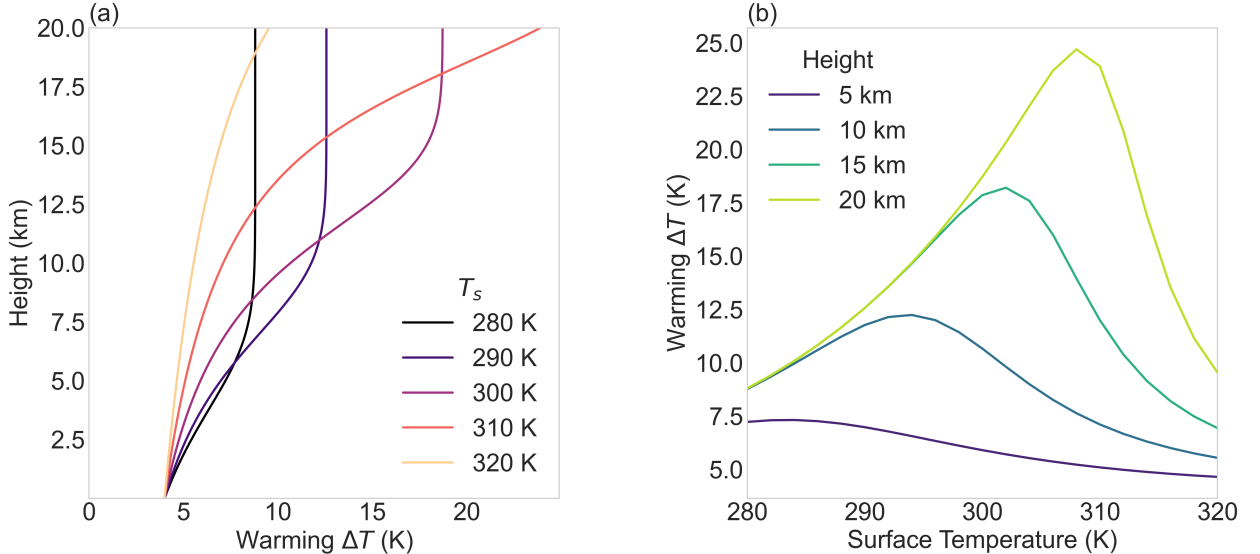
391 We calculate moist-adiabatic profiles numerically by assuming the conservation of saturation moist
392 static energy h^* :

$$h^* = c_{pd}T + gz + L_v q^* \quad (\text{A1})$$

393 where T is temperature, z is height, q^* is the saturation specific humidity, g is the acceleration due
394 to gravity on Earth, c_{pd} is the specific heat of dry air at constant pressure, and L_v is the latent heat
395 of vaporization. We use the Bolton (1980) formula for saturation vapor pressure e^* (Eq. C1). The
396 values we use for all thermodynamic constants are in Table A1.

397 We first calculate surface saturation moist static energy h_s^* for a given surface temperature T_s and
398 surface pressure p_s . We calculate h^* at higher levels in -50 hPa pressure increments. We assume hy-
399 drostatic balance to calculate the height z_{i+1} at the next pressure level p_{i+1} . We solve for T_{i+1} that sat-
400 isfies the condition $h_{i+1}^* = h_s^*$ using Brent's root-finding method (`scipy.optimize.root_scalar`
401 with `method=brentq`).

402 We also show moist-adiabatic warming in height coordinates to demonstrate that the non-
403 monotonicity is not an artifact of the choice of the vertical coordinate (Fig. A1). We follow the
404 same procedure as above except we step to higher levels in 100 m height increments.



405 FIG. A1. (a) Vertical profiles of moist-adiabatic warming to a 4 K surface warming for $T_s = 280, 290, 300,$
 406 310, and 320 K. Warming decreases with initial surface temperature at lower levels while it increases with initial
 407 surface temperature at higher levels. (b) moist-adiabatic warming varies non-monotonically with initial surface
 408 temperature at all levels, e.g. at 5 km, 10 km, 15 km, and 20 km. moist-adiabatic warming peaks at warmer
 409 initial surface temperatures at higher levels.

TABLE A1. Thermodynamic constants used in this study.

Symbol	Description	Value	Units
g	Acceleration due to gravity	9.81	m s^{-2}
c_{pd}	Specific heat of dry air	1005.7	$\text{J kg}^{-1} \text{K}^{-1}$
R_d	Gas constant of dry air	287.05	$\text{J kg}^{-1} \text{K}^{-1}$
R_v	Gas constant of water vapor	461.5	$\text{J kg}^{-1} \text{K}^{-1}$
ϵ	Ratio of gas constants (R_d/R_v)	0.622	dimensionless
p_s	Surface pressure	1000	hPa
L_v	Latent heat of vaporization	2.501×10^6	J kg^{-1}

410

APPENDIX B

411

Sensitivity of Non-monotonicity to Fusion

412 We assess how latent heat of fusion influences the non-monotonicity of moist-adiabatic warming.
 413 Following Flannaghan et al. (2014), we represent freezing following the IFS Cycle 40 documenta-

⁴¹⁴ tion (ECMWF 2022). The fraction of liquid water α varies with T as follows

$$\alpha(T) = \begin{cases} 0, & T \leq T_{\text{ice}} \\ \left(\frac{T - T_{\text{ice}}}{T_0 - T_{\text{ice}}} \right)^2 & T_{\text{ice}} < T < T_0 \\ 1 & T \geq T_0 \end{cases} \quad (\text{B1})$$

⁴¹⁵ where $T_{\text{ice}} = 253.15$ K and $T_0 = 273.15$ K. All condensate is ice below 253.15 K, all condensate is
⁴¹⁶ liquid above 273.15 K, and the transition between the two limits is quadratic.

⁴¹⁷ The saturation vapor pressure e^* is the weighted average over liquid (e_ℓ^*) and ice (e_i^*):

$$e^* = \alpha e_\ell^* + (1 - \alpha) e_i^* \quad (\text{B2})$$

⁴¹⁸ The saturation vapor pressure over liquid and ice is

$$e_{\ell,i}^*(T) = a_1 \exp \left(a_3 \frac{T - T_0}{T - a_4} \right) \quad (\text{B3})$$

⁴¹⁹ where over liquid $a_1 = 611.21$ Pa, $a_3 = 17.502$, $a_4 = 32.19$ K (Buck 1981) and over ice $a_1 =$
⁴²⁰ 611.21 Pa, $a_3 = 22.587$, $a_4 = -0.7$ K (Alduchov and Eskridge 1996).

⁴²¹ The effective latent heat of vaporization $L_e^*(T)$ includes both condensation and fusion:

$$L_e^*(T) = L_v + (1 - \alpha) L_f \quad (\text{B4})$$

⁴²² where $L_f = 0.334 \times 10^6$ J kg⁻¹ is the latent heat of fusion.

⁴²³ Moist adiabats including fusion are obtained by solving for T that conserves the saturation moist
⁴²⁴ static energy with the effective latent heat L_e :

$$h_{\text{fusion}}^* = c_{pd} T + gz + L_e q^* \quad (\text{B5})$$

⁴²⁵ The non-monotonicity of moist-adiabatic warming emerges with or without fusion (compare
⁴²⁶ Fig. 1b and B1a). Fusion introduces a secondary local maximum of warming due to the additional
⁴²⁷ local energy release from fusion (Fig. B1b). When the secondary peak is to the right of the primary

428 peak the T_s of peak warming shifts to colder T_s (points below the 1:1 line in Fig. B1c). As the
 429 secondary peak overlaps with the primary peak, the T_s of peak warming shifts to warmer T_s with
 430 fusion (points above the 1:1 line in Fig. B1c). This effect is largest (6.01 K) at 727 hPa. Since
 431 fusion represents a secondary effect and complicates the analysis, we neglect it in the main analysis.

437 APPENDIX C

438 Sensitivity of Non-monotonicity to Saturation Vapor Pressure Formulas

439 The moist-adiabatic lapse rate depends on the choice of the empirical formula for saturation vapor
 440 pressure e^* . To assess the sensitivity of the non-monotonicity in moist-adiabatic warming to
 441 different empirical fits of $e^*(T)$, we test how the T_s of peak warming varies across three formulas:
 442 Bolton (1980), Goff-Gratch (as described in List 1949), and Murphy and Koop (2005).

443 The Bolton (1980) formula is:

$$e^* = 6.112 \exp\left(\frac{17.67(T - 273.15)}{T - 29.65}\right) \quad [\text{hPa}] \quad (\text{C1})$$

444 The Goff-Gratch formula is:

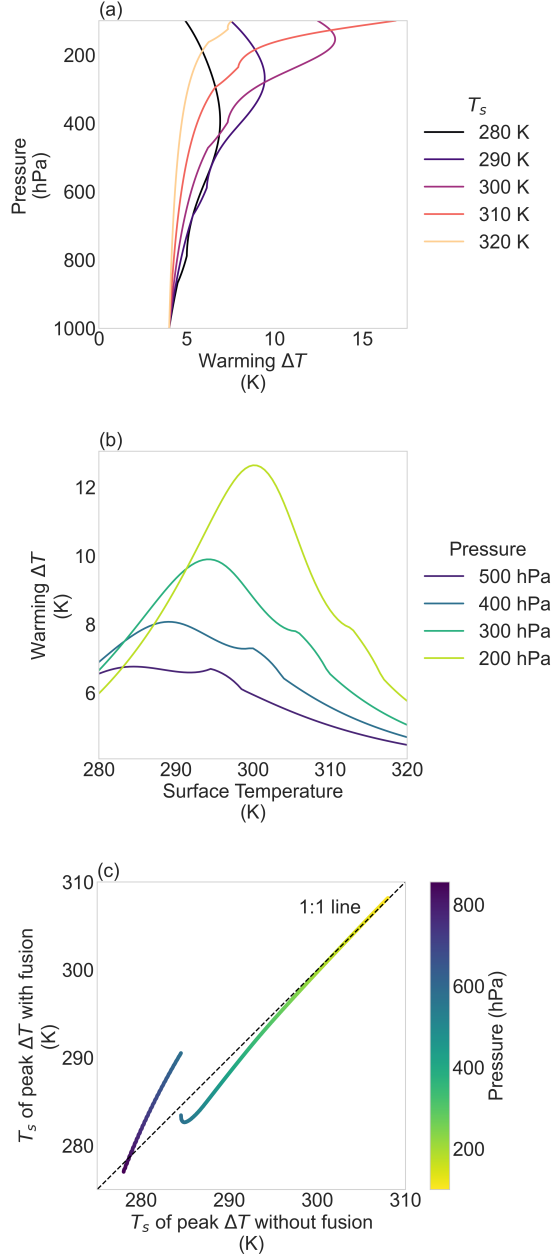
$$\begin{aligned} \log_{10} e^* = & -7.90298 \left(\frac{373.16}{T} - 1 \right) + 5.02808 \log_{10} \left(\frac{373.16}{T} \right) \\ & - 1.3816 \times 10^{-7} \left(10^{11.344(1-T/373.16)} - 1 \right) + 8.1328 \times 10^{-3} \left(10^{-3.49149(373.16/T-1)} - 1 \right) \\ & + \log_{10}(1013.246) \quad [\text{hPa}] \quad (\text{C2}) \end{aligned}$$

445 The Murphy and Koop (2005) formula is:

$$\begin{aligned} \ln e^* = & 54.842763 - \frac{6763.22}{T} - 4.210 \ln T + 0.000367T \\ & + \tanh(0.0415(T - 218.8)) \left(53.878 - \frac{1331.22}{T} - 9.44523 \ln T + 0.014025T \right) \quad [\text{Pa}] \quad (\text{C3}) \end{aligned}$$

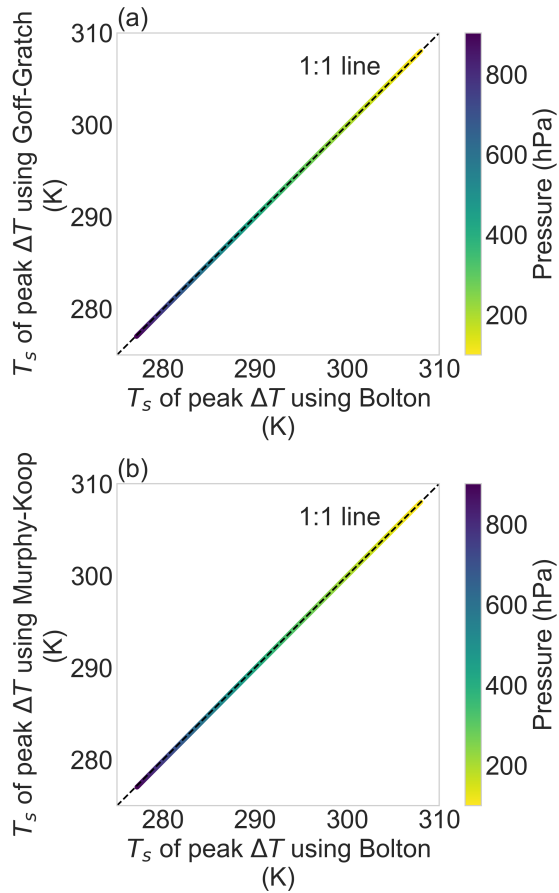
446 where T is in Kelvin for all 3 formulas.

447 Bolton (1980) is sufficiently accurate for the purposes of evaluating the T_s that leads to maxima
 448 in moist-adiabatic warming (Fig. C1). The differences in peak T_s across the three saturation vapor
 449 pressure formulas are small. The largest difference in T_s of peak warming is 0.11 K at 903 hPa



432 FIG. B1. moist-adiabatic warming ΔT for 4 K surface warming including latent heat of fusion. (a) Warming
 433 decreases at lower levels with initial surface temperatures (T_s) while it increases at upper levels with T_s for 280,
 434 290, 300, 310, and 320 K. (b) Warming peaks at warmer T_s at higher levels, e.g. at 500, 400, 300, and 200 hPa.
 435 (c) T_s corresponding to peak warming with and without fusion are comparable at upper levels (> 500 hPa) but
 436 can deviate up to 6.01 K at lower levels (< 500 hPa).

450 between Bolton and Goff-Gratch and 0.16 K at 901 hPa between Bolton and Murphy-Koop. We
 451 choose to use Bolton (1980) in the main analysis due to its simplicity.



452 FIG. C1. (a) T_s corresponding to peak warming using Bolton (1980) and Goff-Gratch saturation vapor pressure
 453 formula are similar (difference is < 0.11 K). (b) Same as (a) but comparing Bolton (1980) and Murphy and Koop
 454 (2005), which also predicts similar T_s of peak warming (difference is < 0.16 K).

455

APPENDIX D

456 Criteria for Moist Greenhouse and Peak CAPE

457 The moist greenhouse transition occurs when high water vapor concentration in the stratosphere
 458 leads to increased photolysis of water vapor and hydrogen escape. The criterion for the onset
 459 of this regime is when the magnitude of the latent to sensible enthalpy at the surface are equal

⁴⁶⁰ (Wordsworth and Pierrehumbert 2013):

$$\frac{L_v q_s^*}{c_{pd} T_s} = 1 \quad (\text{D1})$$

⁴⁶¹ In contrast, peak CAPE corresponds to the surface temperature where the temperature sensitivity
⁴⁶² ratio of latent and sensible enthalpy at the tropopause are equal (which works well for $a \ll 1$,
⁴⁶³ Romps 2016):

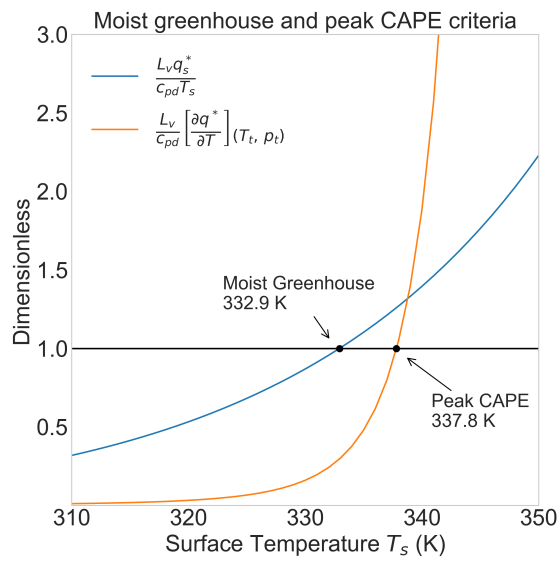
$$\frac{c_{L,t}}{c_{pd}} = \frac{L_v}{c_{pd}} \left. \frac{\partial q^*}{\partial T} \right|_t = 1 \quad (\text{D2})$$

⁴⁶⁴ where the subscript t is the tropopause. Combining Eq. (D2) and Eq. (11) in this paper together
⁴⁶⁵ with Eq. (15) in Romps (2016):

$$\left. \frac{dq^*}{dT} \right|_t \approx \frac{\epsilon}{p_s} \left(\frac{de_t^*}{dT} \exp(\mathcal{A}(T_s - T_t) + \mathcal{B}) - \mathcal{A} e^* \exp(\mathcal{A}(T_s - T_t) + \mathcal{B}) \right) \quad (\text{D3})$$

⁴⁶⁶ where $\mathcal{A} = \frac{c_{pd}}{R_d T_0}$, $\mathcal{B} = \frac{L_v q_s^*}{(1+a) R_d T_0}$, and $T_0 = \frac{T_s + T_t}{2}$. Following Romps (2016) we set $a = 0$ and $T_t = 200$ K
⁴⁶⁷ when calculating Eq. (D3).

⁴⁶⁸ The T_s of the transition to the moist greenhouse regime (332.9 K, where the blue line equals
⁴⁶⁹ 1 in Fig. D1) and peak CAPE (337.8 K, where the orange line equals 1 in Fig. D1) are similar,
⁴⁷⁰ both occurring ≈ 335 K. However, the T_s that satisfy each criteria emerge from nondimensional
⁴⁷¹ numbers that scale differently with T_s . The moist greenhouse criterion proposed by Wordsworth
⁴⁷² and Pierrehumbert (2013) is only a function of surface moist enthalpy partitioning. The peak CAPE
⁴⁷³ criterion is not only a function of surface moist enthalpy but also the tropopause temperature T_t ,
⁴⁷⁴ which is influenced by both moist thermodynamics and radiative transfer (e.g., Held 1982; Hu and
⁴⁷⁵ Vallis 2019). Thus there is no *a priori* expectation that the surface temperatures corresponding to
⁴⁷⁶ these two transitions must coincide across a broad range of planetary climates.



477 FIG. D1. The T_s of the transition to a moist greenhouse regime and peak CAPE are both ≈ 335 K but they
 478 emerge from different criteria. The transition to a moist greenhouse regime corresponds to where the magnitude
 479 of latent and sensible enthalpy are equal (blue line equals 1). Peak CAPE corresponds to where the temperature
 480 sensitivity of latent and sensible enthalpy are equal (orange line equals 1).

481 **References**

- 482 Alduchov, O. A., and R. Eskridge, 1996: Improved magnus form approximation of saturation vapor
483 pressure. *Journal of Applied Meteorology*, **35** (4), 601–609.
- 484 Arakawa, A., and W. H. Schubert, 1974: Interaction of a cumulus cloud ensemble with the
485 large-scale environment, part I. *Journal of the Atmospheric Sciences*, **31** (3), 674–701.
- 486 Bao, J., V. Dixit, and S. C. Sherwood, 2022: Zonal temperature gradients in the tropical free
487 troposphere. *Journal of climate*.
- 488 Bolton, D., 1980: The computation of equivalent potential temperature. *Mon. Weather Rev.*,
489 **108** (7), 1046–1053.
- 490 Buck, A. L., 1981: New equations for computing vapor pressure and enhancement factor. *Journal*
491 *of Applied Meteorology and Climatology*, **20** (12), 1527–1532.
- 492 Byrne, M. P., and P. A. O’Gorman, 2013: Land–ocean warming contrast over a wide range of
493 climates: Convective quasi-equilibrium theory and idealized simulations. *Journal of climate*,
494 **26** (12), 4000–4016.
- 495 Del Genio, A. D., M.-S. Yao, and J. Jonas, 2007: Will moist convection be stronger in a warmer cli-
496 mate?: CONVECTION STRENGTH IN a WARMER CLIMATE. *Geophys. Res. Lett.*, **34** (16).
- 497 ECMWF, 2022: IFS documentation. Accessed: 2025-10-28, <https://www.ecmwf.int/en/publications/ifs-documentation>.
- 498 Emanuel, K. A., 1994: *Atmospheric Convection*. Oxford University Press.
- 500 Flannaghan, T. J., S. Fueglistaler, I. M. Held, S. Po-Chedley, B. Wyman, and M. Zhao, 2014:
501 Tropical temperature trends in atmospheric general circulation model simulations and the impact
502 of uncertainties in observed SSTs. *Journal of Geophysical Research, D: Atmospheres*, **119** (23),
503 13,327–13,337.
- 504 Hansen, J., A. Lacis, D. Rind, G. Russell, P. Stone, I. Fung, R. Ruedy, and J. Lerner, 1984: Cli-
505 mate sensitivity: Analysis of feedback mechanisms. *Climate Processes and Climate Sensitivity*,
506 American Geophysical Union (AGU), 130–163.

- 507 Held, I. M., 1982: On the height of the tropopause and the static stability of the troposphere.
508 *Journal of the Atmospheric Sciences*, **39** (2), 412–417.
- 509 Held, I. M., 1993: Large-scale dynamics and global warming. *Bull. Am. Meteorol. Soc.*, **74** (2),
510 228–242.
- 511 Held, I. M., and K. M. Shell, 2012: Using relative humidity as a state variable in climate feedback
512 analysis. *Journal of climate*, **25** (8), 2578–2582.
- 513 Held, I. M., and B. J. Soden, 2000: Water vapor feedback and global warming. *Annual review of*
514 *energy and the environment*, **25** (1), 441–475.
- 515 Hu, S., and G. K. Vallis, 2019: Meridional structure and future changes of tropopause height and
516 temperature. *Quarterly Journal of the Royal Meteorological Society*, **145** (723), 2698–2717.
- 517 Ingersoll, A. P., 1969: The runaway greenhouse: A history of water on venus. *Journal of the*
518 *atmospheric sciences*, **26** (6), 1191–1198.
- 519 Kasting, J., 1988: Runaway and moist greenhouse atmospheres and the evolution of earth and
520 venus. *Icarus*, **74**, 472–494.
- 521 Keil, P., H. Schmidt, B. Stevens, and J. Bao, 2021: Variations of tropical lapse rates in climate
522 models and their implications for upper tropospheric warming. *Journal of climate*, **34** (24), 1–50.
- 523 Komabayasi, M., 1967: Discrete equilibrium temperatures of a hypothetical planet with the
524 atmosphere and the hydrosphere of one component-two phase system under constant solar
525 radiation. *Journal of the Meteorological Society of Japan*, **45** (1), 137–139.
- 526 Levine, X. J., and W. R. Boos, 2016: A mechanism for the response of the zonally asymmetric
527 subtropical hydrologic cycle to global warming. *J. Clim.*, **29** (21), 7851–7867.
- 528 List, R. J., 1949: Smithsonian meteorological tables. *Smithsonian miscellaneous collections*, **114**,
529 1–521.
- 530 Miyawaki, O., Z. Tan, T. A. Shaw, and M. F. Jansen, 2020: Quantifying key mechanisms that
531 contribute to the deviation of the tropical warming profile from a moist adiabat. *Geophys. Res.*
532 *Lett.*, **47** (20), e2020GL089136.

- 533 Murphy, D. M., and T. Koop, 2005: Review of the vapour pressures of ice and supercooled water
534 for atmospheric applications. *Quarterly journal of the Royal Meteorological Society. Royal*
535 *Meteorological Society (Great Britain)*, **131 (608)**, 1539–1565.
- 536 Neelin, J. D., and I. M. Held, 1987: Modeling tropical convergence based on the moist static energy
537 budget. *Mon. Weather Rev.*, **115 (1)**, 3–12.
- 538 O’Gorman, P. A., 2015: Precipitation extremes under climate change. *Current climate change*
539 *reports*, **1 (2)**, 49–59.
- 540 Riehl, H., and J. S. Malkus, 1958: On the heat balance of the equatorial trough zone. *Geophysica*,
541 **6 (3-4)**.
- 542 Romps, D. M., 2016: Clausius–Clapeyron scaling of CAPE from analytical solutions to RCE. *J.*
543 *Atmos. Sci.*, **73 (9)**, 3719–3737.
- 544 Santer, B. D., and Coauthors, 2005: Amplification of surface temperature trends and variability in
545 the tropical atmosphere. *Science*, **309 (5740)**, 1551–1556.
- 546 Seeley, J. T., and D. M. Romps, 2015: Why does tropical convective available potential energy
547 (CAPE) increase with warming? *Geophysical research letters*, **42 (23)**, 10,429–10,437.
- 548 Seeley, J. T., and D. M. Romps, 2016: Tropical cloud buoyancy is the same in a world with or
549 without ice. *Geophysical research letters*, **43 (7)**, 3572–3579.
- 550 Shaw, T. A., and O. Miyawaki, 2025: Moist adiabatic scaling explains mean and fast upper-level jet
551 stream wind response to climate change. *Geophysical research letters*, **52 (20)**, e2025GL118 315.
- 552 Shaw, T. A., and A. Voigt, 2016: What can moist thermodynamics tell us about circulation shifts
553 in response to uniform warming? *Geophysical research letters*, **43 (9)**, 4566–4575.
- 554 Singh, M. S., and P. A. O’Gorman, 2013: Influence of entrainment on the thermal stratification
555 in simulations of radiative-convective equilibrium. *Geophysical research letters*, **40 (16)**, 4398–
556 4403.
- 557 Singh, M. S., and P. A. O’Gorman, 2015: Increases in moist-convective updraught velocities with
558 warming in radiative-convective equilibrium. *Quarterly Journal of the Royal Meteorological*
559 *Society*, **141 (692)**, 2828–2838.

- 560 Vallis, G. K., P. Zurita-Gotor, C. Cairns, and J. Kidston, 2015: Response of the large-scale structure
561 of the atmosphere to global warming. *Quart. J. Roy. Meteor. Soc.*, **141** (690), 1479–1501.
- 562 Wing, A. A., K. A. Reed, M. Satoh, B. Stevens, S. Bony, and T. Ohno, 2018: Radiative–convective
563 equilibrium model intercomparison project. *Geoscientific Model Development*, **11** (2), 793–813.
- 564 Wordsworth, R. D., and R. T. Pierrehumbert, 2013: WATER LOSS FROM TERRESTRIAL
565 PLANETS WITH CO₂-RICH ATMOSPHERES. *The Astrophysical Journal*, **778** (2), 154.